The X-ray and ultraviolet absorbing outflow in 3C 351

THE ASTROPHYSICAL JOURNAL, 434:493–502, 1994 October 20

THE X-RAY AND ULTRAVIOLET ABSORBING OUTFLOW IN 3C 351

SMITA MATHUR,[1] BELINDA WILKES, MARTIN ELVIS, AND FABRIZIO FIORE
Harvard-Smithsonian Center for Astrophysics, 60 Garden Street, Cambridge, MA 02138
Received 1994 January 3; accepted 1994 April 27

ABSTRACT

3C 351 ($z = 0.371$), an X-ray–"quiet" quasar, is one of the few quasars showing signs of a "warm absorber" in its X-ray spectrum; i.e., partially ionized absorbing material in the line of sight whose opacity depends on its ionization structure. The main feature in the X-ray spectrum is a K-edge due to O VII or O VIII. 3C 351 also shows unusually strong, blueshifted, associated, absorption lines in the ultraviolet (Bahcall et al. 1993) including O VI ($\lambda\lambda$1031, 1037). This high ionization state strongly suggests an identification with the X-ray absorber and a site within the active nucleus.

In this paper we demonstrate that the X-ray and UV absorption is due to the same material. This is the first confirmed UV/X-ray absorber. Physical conditions of the absorber are determined through the combination of constraints derived from both the X-ray and UV analysis. This highly ionized, outflowing, low-density, high–column density absorber situated outside the broad emission line region (BELR) is a previously unknown component of nuclear material.

We rule out the identification of the absorber with a BELR cloud as the physical conditions in the two regions are inconsistent with one another. The effect of the X-ray quietness and IR upturn in the 3C 351 continuum on the BELR is also investigated. The strengths of the high-ionization lines of C IV λ1549 and O VI λ1034 with respect to Lyα are systematically lower (up to a factor of 10) in the material ionized by the 3C 351 continuum as compared to those produced by the "standard" quasar continuum, the strongest effect being on the strength of O VI λ1034. We find that for a 3C 351-like continuum, C III] λ1909 ceases to be a density indicator.

Subject headings: quasars: absorption lines — quasars: individual (3C 351) — ultraviolet: galaxies — X-rays: galaxies

1. INTRODUCTION

A minority of AGNs show optical and ultraviolet absorption lines within the profiles of their broad emission lines (Ulrich 1988). While this ionized absorbing material must be associated with the active nucleus, there is no accepted model for it (see, e.g., Kolman et al. 1993). Similarly, many AGNs, mostly Seyfert galaxies exhibit strong low-energy X-ray cutoffs (e.g., Turner & Pounds 1989) due to "cold" material in their nuclei, also with no accepted identification. The possibility of linking these two types of absorbers has not seemed promising to date (Ulrich 1988). However, recent observations of X-ray ionized ("warm") absorbers promise to change this situation, 3C 351 provides a particularly good opportunity.

3C 351 ($z = 0.371$) is one of the few quasars showing signs of a warm absorber in its X-ray spectrum; i.e., a partially ionized absorbing material in the line of sight whose opacity depends on its ionization structure (Fiore et al. 1993, hereafter Paper I). The main feature in the X-ray spectrum is a K-edge due to O VII or O VIII. 3C 351 also shows unusually strong, associated, absorption lines in the ultraviolet (Bahcall et al. 1993) including O VI ($\lambda\lambda$1031, 1037), strongly suggesting an identification with the X-ray absorber, and a site within the active nucleus.

In this paper we search for, and find, a model for the absorber which is consistent with both the X-ray and UV data. We reanalyze the X-ray and UV data with this aim in mind (§ 2). In order to produce self-consistent models, we find that use of the observed (ionizing) continuum of 3C 351, rather than a generic quasar continuum is critical (§ 4). We find that the UV absorption-line clouds (§ 3), but not the broad emission line region (BELR) clouds (§ 4), can cause the X-ray absorption. We derive the physical characteristics of this outflowing material (§ 3) and consider why a previous similar attempt to identify an X-ray absorber with a strong UV absorber in a different AGN was not successful (§ 5).

2. X-RAY, ULTRAVIOLET, AND OPTICAL DATA

2.1. *X-Ray Spectrum*

The details of the X-ray observations, extraction of the source pulse height spectrum, and its analysis are presented in Paper I. This analysis concludes that an ionized ("warm") absorber is present, whose dominant feature is a strong O VII/O VIII absorption edge. The inferred parameters of the best-fit X-ray spectrum (the total column density N_H and the ionization parameter U, defined as the dimensionless ratio of ionizing photon to baryon density) depend critically on the assumed ionizing continuum which in Paper I was assumed to be a simple power law between 10 μm and 5 MeV. To investigate the extent of this dependence, we refitted the X-ray spectrum using the observed 3C 351 continuum (§ 2.3) to ionize the absorber. Since the shape of the continuum in the extreme ultraviolet is unknown, a broken power-law model was used with the break energy varied from the unobserved EUV range to well within the PSPC range: 0.07 keV, 0.37 keV, and 0.7 keV. The slope ($f_\nu \propto \nu^{-\alpha}$) in the soft energy range (α_1) was fixed by the observed flux in the UV at one end and the break energy at the other. The slope, α_2, above the break energy was fixed at 1, typical for lobe-dominated, radio-loud quasars (Shastri et al. 1993). The resulting parameters are given in Table 1. The best-fit spectrum, folded through the instrument response and com-

[1] Internet: smita@cfa.harvard.edu.

TABLE 1

ROSAT TWO-POWER-LAW SPECTRAL FITS

Break Energy (keV) (Fixed)	α_1 (Fixed)	α_2 (Fixed)	χ^2[a]	N_H[b] (10^{22} cm^{-2})	log U[b]
0.07	4.7	1	24.73	$1.8^{+0.4}_{-0.3}$	$1.08^{+0.12}_{-0.08}$
0.37	2.45	1	29.82	1.4 ± 0.3	$0.83^{+0.13}_{-0.09}$
0.7	2.16	1	31.66	$1.0^{+0.4}_{-0.2}$	$0.04^{+0}_{-0.35}$

[a] For 21 degrees of freedom.
[b] Errors are 1 σ for 2 degrees of freedom.

pared with the data, is shown in Figure 1. The fits gave $\chi^2 = 24.7$, 29.8, and 31.7, respectively, for the three models for 27 degrees of freedom. A χ^2 of 31.7 is unacceptably large (probability of 25%) so a break at a lower energy (0.37 keV or less) is preferred. The difference in the break energy in the two acceptable models results in a factor of two differences in the best fit values of the absorbing column density ($N_H = 1$–2×10^{22} atoms cm^{-2}), and in the ionization parameter U of the warm absorber (log $U = 0.78$–1.08). The best-fit ionization parameter differs by a factor of $\sim$30 from that for a single power law (log $U = -1$ to -0.7), while the column density is similar ($N_H = 1$–4×10^{22} atoms cm^{-2}) (Paper I).

2.2. *Ultraviolet and Optical Spectra*

3C 351 was also observed by *HST* as a part of the Quasar Absorption Lines Key Project (Bahcall et al. 1993). By a fortunate coincidence, the *HST* ultraviolet observations were quasi-simultaneous with the X-ray observations (*ROSAT*: 1991 October 28–30; *HST*: 1991 October 22). The spectra were obtained from the *HST* archive and analyzed using IRAF. An unusually strong metal line absorption system (Figs. 2*a*–2*d*) is observed at $z = 0.3646$ (Bahcall et al. 1993) and contains the high ionization doublets of O VI, N V, and C IV and the Lyman series Lyα, Lyβ, Lyγ (blended with another Lyα line at $z = 0.092$), and Lyδ. Bahcall et al. (1993) suggested that an associated cluster of galaxies is responsible for the UV absorber. However, a deep image of this field (Ellingson et al. 1994) shows that there are no associated galaxies. We conclude that the UV absorber is associated with the quasar itself.

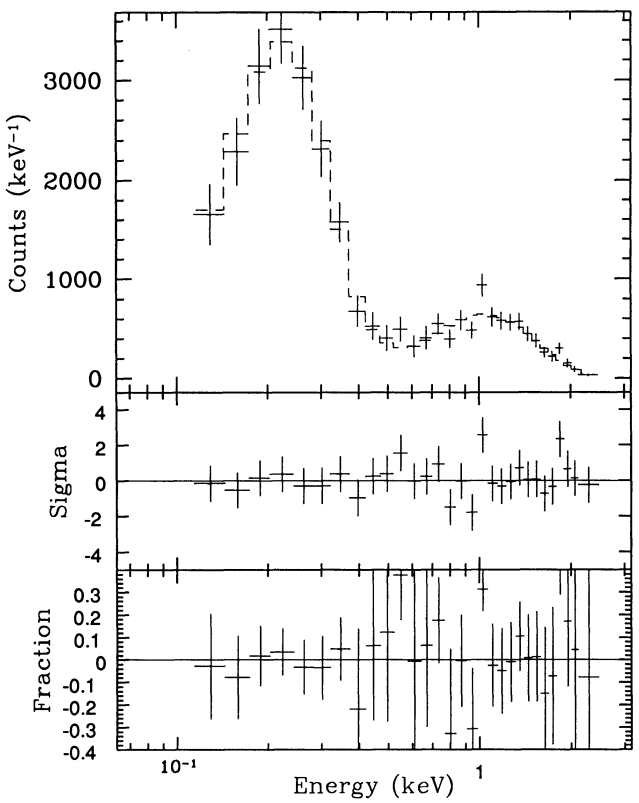

FIG. 1.—The best-fit X-ray spectrum. The data plus the folded model ($E_{break} = 0.37$ keV, $N_H = 1.4 \times 10^{22}$ cm^{-2}, $U = 6.7$) are shown in the top panel; residuals after subtracting the best-fit model are shown in the lower two panels.

Table 2 lists the equivalent widths (EW), and full width at half-maximum (FWHM), of the absorption lines in the $z = 0.3646$ system given by Bahcall et al. with the exception of C IV and N V which we remeasured. The automatic algorithm used by Bahcall et al. to identify the absorption lines finds a weak C IV doublet at 2112.8 and 2116.6 Å (EW = 0.26 Å and 0.12 Å, respectively) but leaves the strong (EW = 3.09 Å), broad (FWHM = 8.58 Å) line at 2114.5 Å unidentified. Inspection of the spectrum (Fig. 2*c*) shows that the C IV absorption doublet is not clearly resolved, which is not surprising given the typical FWHM (3–4 Å) of the absorption lines in this system. If we assume that the whole absorption for this broad system (FWHM = 8.58 Å) at 2114 Å is due to an unresolved C IV blend (1549.1 Å), the redshift is then 0.3646, in agreement with the rest of the system. We use this larger EW in our modeling.

Measurements of absorption lines embedded in a quasar's strong emission lines are prone to large uncertainties since their "continuum" is actually the unknown profile of an emission line. This can be seen in Figure 2 where the associated absorber covers most of the blue wing of both O VI and C IV emission lines. For the N V absorption doublet, situated in the blue wing of N V and red wing of Lyα, the problem is even greater. The published values of the N V ($\lambda\lambda$1238, 1242) absorption line EWs are 1.60 Å and 1.63 Å using a continuum defined by a cubic spline fit to a number of discrete continuum points (Schneider et al. 1993). As can be seen in Figure 2, the resulting Lyα emission line profile is symmetric allowing for little or no N V emission. We measured the N V absorption using several plausible continuum levels and conclude $\sim$40%

TABLE 2

UV EMISSION AND $z = 0.3646$ ABSORPTION-LINE PARAMETERS

Line Identification	λ_{obs} (Å)	EW_{obs}[b] (Å)	FWHM (Å)
A. Absorption[a]			
C IV λ1549	2113	3.09	8.58
N V λ1238	1690.74	1.60[c]	3.22
N V λ1242	1695.67	1.63[c]	3.44
Lyα	1658.92	3.54[c]	4.46
O VI λ1031	1408.34	2.73	3.09
O VI λ1037	1416.39	1.99	2.85
B. Emission			
C III] λ1909	2614.6	18.5	25.0
C IV λ1549	2121.98	68.2	32.2
Lyα/N V	1664.11	60.5	31.6
O VI $\lambda\lambda$1031, 1037	1426.14	6.8	23.0

[a] From Bahcall et al. 1993 except for the uncertainties in EWs.
[b] Uncertainties are $\sim$10% except where noted.
[c] Uncertainties are estimated to be $\sim$40%.

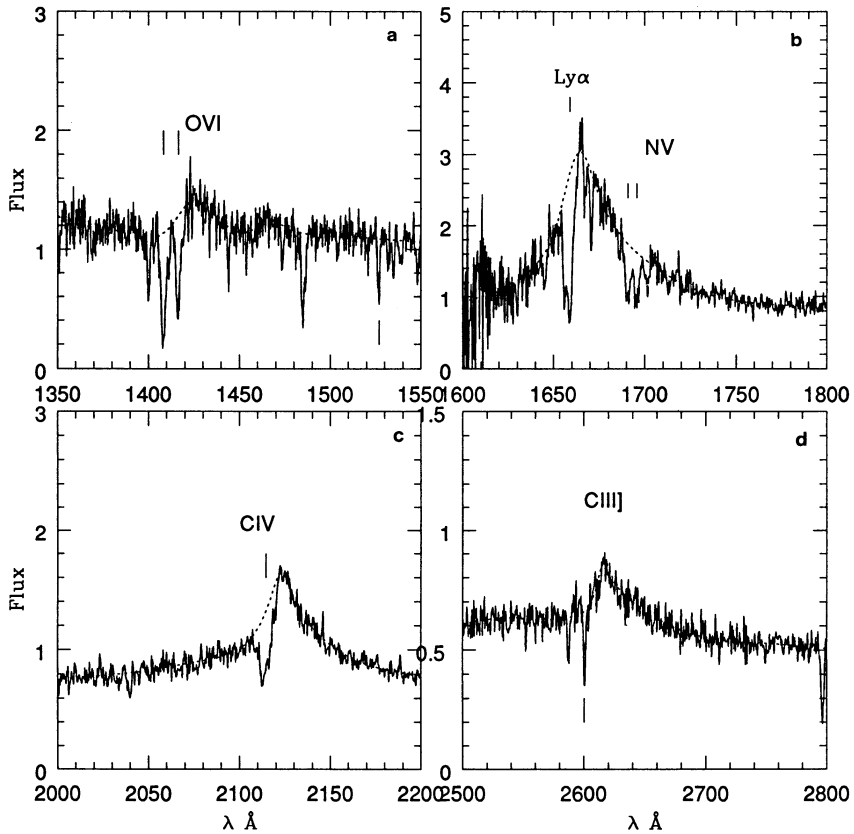

FIG. 2.—The *HST* UV spectrum: (*a*) O VI, (*b*) Lyα/N V, (*c*) C IV, (*d*) C III]. Flux is in the units of 10^{-14} ergs s^{-1} cm^{-2} $Å^{-1}$. The dotted line is the continuum defined in Bahcall et al. (1993). The prominent emission lines are labeled. The absorption lines in $z = 0.3646$ system are marked above the spectrum, and the Galactic absorption lines are marked below the spectrum.

uncertainties which we take into account in our modeling. A similar level of uncertainty was deduced for the Lyα absorption line ($z = 0.3646$) due to blending with another Lyα absorption line ($z = 0.3621$) and the highly uncertain blue wing of the Lyα profile.

The FWHM of these absorption lines in the $z = 0.3646$ system ranges from 2.08 Å to 6.26 Å (rest frame). This implies a maximum value of the velocity spread parameter "b" to be < 600–1200 km s^{-1} (see § 4 for further details).

No lines from the low-ionization ions of C II, N I, N II, O I, Si II, Al II, and Fe II are present (equivalent widths $\lesssim 0.4$ Å) (Bahcall et al. 1993). Also, ground-based observations by Boissé et al. (1992) show no $z = 0.3646$ Mg II absorption doublet, giving an upper limit of 0.1 Å to its equivalent width.

Bahcall et al. (1993) do not report emission-line strengths. In order to see whether the high-ionization emission-line clouds could produce the X-ray absorption, equivalent widths and fluxes were measured for lines of Lyman-α, C IV λ1549, C III] λ1909, and O VI λ1034 using local continuum estimates, and the results are given in Table 2. As discussed above, the spectral lines show strong absorption features. Lyman-α is also blended with emission lines of Si II λ1260 and N V λ1240, and the Si II λ1537, Ne V λ1575 features cannot be separated from the C IV λ1549 emission line. Apart from N V λ1240, which is a strong contaminant, these lines are weak and are not expected to exceed ~10% of the line. In all cases the weaker lines were included in the line strengths predicted by photoionization models so that a proper comparison with observed lines could be made. The emission line fluxes were corrected for the absorption-line systems using the EWs in Table 2.

3C 351 was also observed in the ultraviolet by *IUE*. Kinney et al. (1991) have published an optimally extracted, "co-added" spectrum of 3C 351. As a consistency check, the co-added spectrum of 3C 351 was obtained from the *IUE* archive and analyzed to measure the strengths of the emission lines. The equivalent widths of the lines were found to be consistent with those measured from the *HST* spectra.

2.3. *Observed Energy Distribution of 3C 351*

The thermal and ionization structure of a photoionized gas cloud is dependent on the strength and shape of the complete millimeter–X-ray incident continuum. Most photoionization studies to date have used a standard continuum shape (e.g., Mathews & Ferland 1987), neglecting this as a variable, due to the general lack of good continuum observations. However, 3C 351 has a well-observed radio–X-ray continuum which is significantly different from the standard continuum, allowing us to carry out more realistic modeling of photoionized gas in its vicinity.

Figure 3 shows the observed continuum of 3C 351 (*solid line*; data from Elvis et al. 1994). The X-ray slope α ($f_\nu \propto \nu^{-\alpha}$) is not well constrained due to the presence of the ionized absorber. We use two extreme values of α for radio loud quasars (0.0, 1.0) (Wilkes & Elvis 1987) to investigate its effect on the resulting emission line strengths (Fig. 3). We have extrapolated our best-fit spectrum into the submillimeter region with $\alpha = -5/2$

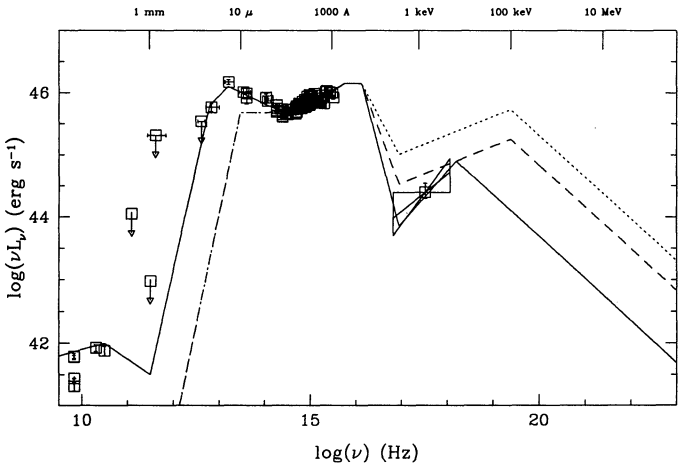

FIG. 3.—The 3C 351 (PG 1704+608) continuum. *Solid line*: the best-fit continuum; *dashed line*: "standard" continuum; and *dotted line*: average X-ray continuum for radio-loud quasars. The bow shows our adopted limits to the X-ray slope α (see text).

(appropriate for synchrotron self-absorption) and the core radio component is smoothly joined onto it. The exact point when the two components join is not well defined but small differences here do not change our results significantly. The short dashed line is the AGN continuum defined in CLOUDY (Ferland 1991) which we shall call the "standard continuum." This standard continuum is similar to that used by Mathews & Ferland (1987) with the exception that the spectral index is changed from -1 to $-5/2$ for frequencies below the millimeter break. The dotted line shows the average X-ray continuum for the radio-loud quasars. All the continua are normalized to match the observations in the optical/UV.

The observed 3C 351 continuum and the standard continuum differ significantly in the X-ray, IR, and radio regions (Fig. 3). 3C 351 is X-ray–"quiet," i.e. it has a factor of ~ 5 lower X-ray flux than the average radio-loud quasar: the effective optical–to–X-ray slope α_{OX} for 3C 351 is 1.6, as compared to $\alpha_{OX} = 1.3$ for an average radio-loud quasar (Wilkes et al. 1994). The weak flux in the X-ray is not due to X-ray variability or to the effect of the ionized absorber (Paper I). 3C 351 also shows a clear upturn in the IR at ~ 1 μm, turning over again at ~ 25 μm. IR and radio emission can produce large amounts of free-free heating which can influence the relative strength of emission lines (Ferland & Persson 1989). The 1.3 mm observations by Antonucci & Barvainis (1993) are critical to the thermal balance since they strongly limit the extrapolation of the IR continuum. If the IR points are smoothly joined onto the radio, then the resulting continuum produces a large amount of free-free heating and unacceptably strong C IV λ1549 emission relative to Lyα. If, instead, the 1.3 mm observations are used, the slope in the submillimeter region is constrained to $-5/2$, similar to that of radio-quiet quasars (Chini, Kreysa, & Biermann 1989). This provides another argument in favor of the Antonucci & Barvainis (1993) hypothesis that the IR and radio emission comes from two distinct components and must arise at different locations. In § 4 we investigate the effect of using the 3C 351 continuum on the physical conditions in photoionized gas clouds and so on the resulting emission line strengths.

3. THE X-RAY ABSORBER AS THE UV ABSORBER

Table 2A gives the EW and FWHM of the absorption lines in the $z = 0.3646$ system. The existence of highly ionized O VI lines is particularly intringuing given the O VII absorption edge seen in soft X-rays (§ 2). If the two absorbers are identical, then the X-ray and UV constraints would allow us to solve for a consistent model for both the UV lines and the X-ray absorber.

In the context of photoionization models, we look for a consistent solution for the ionization state of an absorbing gas cloud satisfying both the X-ray and UV constraints. All the photoionization calculations were made using G. Ferland's CLOUDY software (Ferland 1991). Photoionization models predict $f_{\rm ion}$ given the input continuum, column density, number density ($n_{\rm H}$), and the ionization parameter (U) of the gas, where $f_{\rm ion}$ is the fractional abundance of an element in a given ionization state. For the best-fit parameters of the X-ray absorber (see § 2.1, Table 1), $f_{\rm ion}$ was calculated for the ions O VI, N V, C IV, and H I. Assuming a solar abundance of elements relative to hydrogen and using the total $N_{\rm H}$ from the X-ray analysis, the column density of each ion, $N_{\rm ion}$, was then derived. For example, $f_{\rm O\ VI}$, the fraction of oxygen in the O VI state of ionization, is 0.03 for the continuum model with break energy at 0.37 keV (§ 2.1). Given a solar abundance of oxygen relative to hydrogen (8.51×10^{-4}; Grevesse & Anders 1989) and using the total $N_{\rm H}$ (1.4×10^{22} cm^{-2}), the column density of O VI is $N_{\rm O\ VI} = 3 \times 10^{17}$ cm^{-2}. $N_{\rm ion}$ for the other ions has been derived similarly. These model values are listed in Table 3.

A measured column density for each ion of the UV absorber was derived from the line EW with a standard curve-of-growth analysis (e.g., Spitzer 1978). Figure 4 shows curves of growth for "b" values ranging from 80 to 130 km s^{-1}, where "b" is the velocity spread parameter. Abscissa is log ($N\lambda f$), where N is the column density of an ion and $N\lambda$ has the dimension cm^{-1}. f is the oscillator strength of the transition. Values of f are taken from Wiese, Smith, & Glennon (1966). The lower limit to the column density of an ion is obtained from the linear part of the curve of growth, e.g., for the O VI doublet transition $N_{\rm O\ VI} > 1.7 \times 10^{15}$ cm^{-2}. Small values of "b" imply unacceptably large column densities ("b" = 4 km s^{-1} gives $N_{\rm O\ VI} \sim 10^{27}$ cm^{-2}), making the absorbing material optically thick to Thompson scattering. The maximum value of b is $\sim$600–1200

TABLE 3

COMPARISON OF COLUMN DENSITIES IN MODEL AND DATA

ION	log $N_{\rm ion}$ (Measured)[a]	log $N_{\rm ion}$ (Model) $E_{\rm Break} = 0.07$ keV	$E_{\rm Break} = 0.37$ keV	$E_{\rm Break} = 0.7$ keV
O VI	17.5–18.0	17.5	17.5	18.3
N V	15.3–15.8	15.7	15.8	16.8
C IV	15.9–16.1	15.9	15.9	17.3
H I (Lyα)	15.4–17.4	15.3	15.6	16.5

[a] Assuming $b = 110$ km s^{-1}.

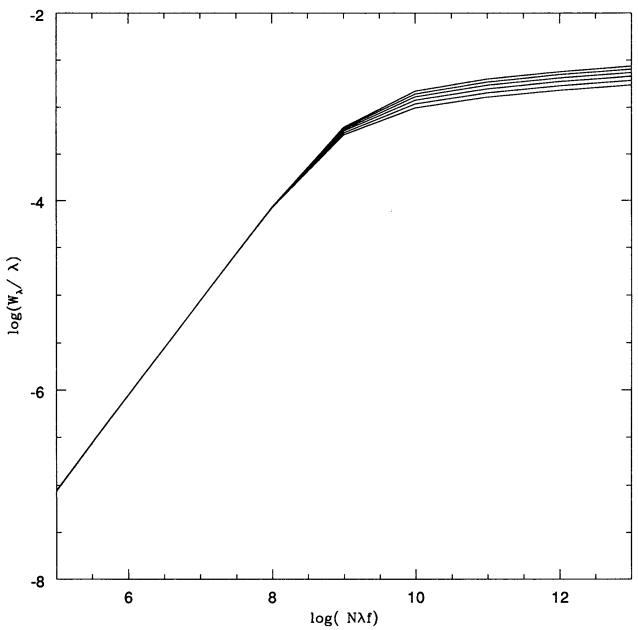

FIG. 4a

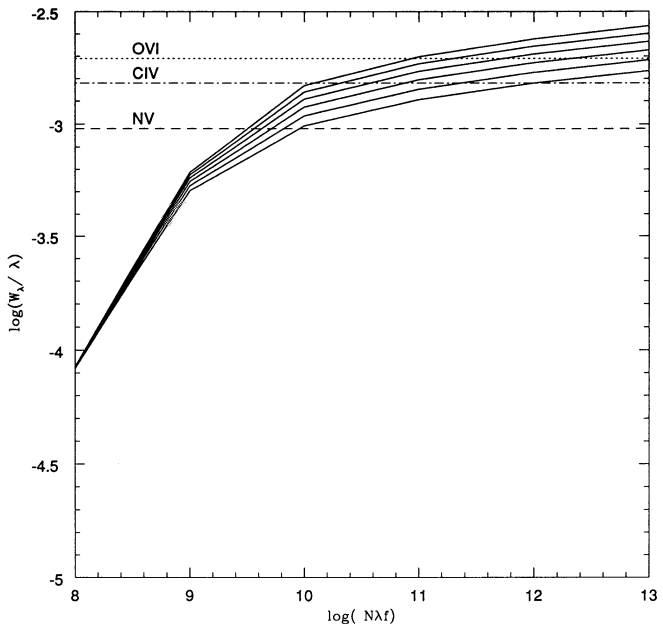

FIG. 4b

FIG. 4.—(*a*) The curve of growth for "*b*" values ranging from 80 to 130 km s^{-1} in steps of 10. *f* is the oscillator strength of the transition and $N\lambda$ has the dimension cm^{-1}. (*b*) A part of (*a*) expanded. Observed values of W_λ/λ for O VI λ1031, C IV λ1549, and N V λ1242 are marked by the horizontal lines.

km s^{-1} given by the observed line widths (see § 2.2). Higher resolution data are needed to allow *b* to be directly measured and then *b* and $N_{\rm ion}$ to be fitted independently. Given the observational limits, we find that a value of $b \sim 105$–115 km s^{-1} gives consistent solutions to the X-ray and UV line constraints (Table 3), a value $b = 110$ km s^{-1} was adopted. The measured column density of O VI is then $N_{\rm O\,VI} = 3 \times 10^{17}$ cm^{-2} consistent with that derived from photoionization model.

Table 3 compares the column densities of each ion derived from the UV line analysis to those predicted by the photoionization models for different values of X-ray spectral break energy. A consistent solution was obtained for all the UV lines: O VI, C IV, N V, and Lyα (Fig. 4*b*). The range in the measured values of column density is due to the uncertainty in the equivalent width measurements. For X-ray continua with break energies at 0.07 and 0.37 keV, the match provided by the models is good to better than 5% for C IV and O VI and consistent for N V and Lyα. As noted in § 2.2, the heavy blending of Lyα and N V results in a large uncertainty in the continuum level and so in the resulting equivalent width of N V. Thus the inferred range of $N_{\rm N\,V}$ is large (15.3–15.8). Similarly, the uncertainty in $N_{\rm H\,I}$ is large (15.4–17.4) due to the large uncertainty in the measurement of equivalent width of Lyα absorption line (§ 2.2).

In a highly ionized system such as this, magnesium is highly ionized (Mg VI and higher) leaving no magnesium in the Mg II state ($\log f_{\rm Mg\,II} < -30$), and thus Mg II absorption should not occur. The same is also true for the low ionization ions of C II, N I, N II, O I, Si II, Al II, and Fe II. This is consistent with the observations (see § 2.2).

For the X-ray model with break energy at 0.7 keV, the inferred parameters for the UV absorber are inconsistent with the parameters of the X-ray absorber (Table 3). If the X-ray absorber is indeed the UV absorber, for which the above evidence is compelling, then the break in the X-ray power law must be at lower energies. We note that this model also has the highest χ^2 (31.66 for 27 dof) among all the three models (§ 2) and the X-ray fit is unacceptable (Table 1). A break at lower energies (~0.37 keV or less) is thus preferred by both X-ray and UV data.

We conclude that in 3C 351 the X-ray and UV absorbers are one and the same.

3.1. *The Physical Characteristics of the Absorber*

Since the X-ray absorber is strongly identified with the UV absorber, constraints from both UV and X-ray data can be combined to derive its physical properties. These properties describe a component of nuclear material not previously recognized. We have already shown that the absorber has high $N_{\rm H}$ (1–1.8 × 10^{22} cm^{-2}), and high *U* (log $U = 0.78$–1.08). We tested a range of density from 10^3 to 10^{11} cm^{-3} in the photoionization models and found that there is no significant change in the values of fractional ionization, so the density is not constrained directly.

The absorption lines are blueshifted with respect to the high ionization emission lines by ~2000 km s^{-1}. The high ionization lines themselves generally show blueshifts of 1000–2000 km s^{-1} (Espey et al. 1989) relative to the Balmer lines. An MMT spectrum taken in 1991 September shows that the high-ionization emission lines of 3C 351 are blueshifted by ~1050 km s^{-1} relative to [O III] λ4959, implying an outflow velocity for the absorber of ~3050 km s^{-1} in the quasar rest frame.

The UV absorption troughs extend through the emission lines down below the continuum level (Fig. 2) requiring that both the continuum-emitting region and the BELR are at least partially covered by the absorber. This places the absorber outside the BELR. Scaling from the BELR size deduced from the reverberation mapping of NGC 5548 (Clavel et al. 1991) by the square root of 3C 351 luminosity ($L_{\rm 3C\,351} = 2 \times 10^3$ $L_{\rm N5548}$, $r_{5548} = 10$ lt-days) yields a distance of the BELR from the central continuum of ~$\frac{1}{3}$ pc. So the distance of the absorber is $r_{\rm abs} \gtrsim \frac{1}{3}$ pc. The larger ionization parameter and

larger radial distance compared to the BELR imply a lower density for the absorber. The radial distance of the ionized absorber is given by $r_{abs} = (Q/4\pi U n_H c)^{1/2}$, where Q is the number of ionizing photons. For the best-fit parameters of the warm absorber this gives $r_{abs} = 5 \times 10^{19} n_5^{-1/2}$ cm, where n_5 is the number density in units of 10^5 cm^{-3}. Hence the density of the absorber must be $\lesssim 5 \times 10^7$ cm^{-3}. This low density in combination with the large column density ($1–2 \times 10^{22}$ cm^{-2}), implies a depth for the absorber, $\gtrsim 2 \times 10^{14}$ cm. Given the above density and physical depth, this leads to a mass for the absorber of $\gtrsim 10^3 M_\odot$ for a covering factor of unity.

The depth of the Lyα absorption line (2.06×10^{-14} ergs^{-1} cm^{-2} Å^{-1}) exceeds the continuum level (0.77×10^{-14} ergs^{-1} cm^{-2} Å^{-1}) (Fig. 2*b*) implying that the absorber covers most ($\gtrsim$60%) of the BELR. However we note that the different lines indicate different percentages of the emission lines being covered, e.g., assuming that 100% continuum source is covered, the depth of the O VI line imples that the BELR may not be covered.

Further constraints come from the fact that a cloud with these physical properties exposed to the quasar continuum radiation would necessarily emit line radiation. If the covering factor of the absorption-line clouds is not small, the line ratios to Lyα would be much larger than the observed ones, as discussed in § 4.2. The contribution of the absorbing clouds to the total emission line flux should be $<10\%$ to be consistent with the observed line ratios. The covering factor of such clouds must then be low (<0.01).

The radiation pressure experienced by the warm absorber is easily sufficient to accelerate it to outflow velocities of a few thousand km s^{-1}, as shown by Turner et al. (1993). The effective Eddington limit for the warm absorber gas is given by $L_{Edd}^{eff} = L_{Edd} \times \sigma_T/\sigma_{eff}$, where σ_T is the Thomson cross section and σ_{eff} is the effective cross section including photoelectric absorption. σ_{eff} is defined such that

$$e^{-\sigma_{eff} N_H} \int_E f(E) dE = \int_E f(E) e^{-\sigma(E) N_H} dE ,$$

where $f(E)$ is the transmitted flux at energy E and $\sigma(E)$, the absorption cross section at energy E, is $\sum_{ion} \sigma_{ion}(E) f_{ion} A$(atom/H). σ_{eff} is $\sim 1.4 \times 10^{-23}$ for a break energy of 0.37 keV. Thus $L_{Edd}^{eff} = 4.7 \times 10^{-2} L_{Edd}$. A quasar (or a Seyfert galaxy) emitting not too far below its Eddington luminosity must necessarily accelerate a warm absorber outward due to its radiation pressure. This is consistent with the blueshift seen in the UV absorber. Turner et al. (1993) reached a similar conclusion for the ionized absorber in NGC 3783.

The corresponding mass-loss rate is $0.05 < \dot{M} < 5\ M_\odot$ yr^{-1} for covering factors between 1% and unity. This is comparable to the accretion rate needed to power the central continuum source, $\dot{M}_{accretion} = 2\ M_\odot$ yr^{-1} for an efficiency of 0.1. Thus the net amount of inflowing matter must be at least a factor of 2 larger than the accretion rate. The outflow implies a kinetic luminosity of $(0.06–6) \times 10^{42}$ ergs s^{-1}, which is only 10^{-5} to 10^{-3} of the radiative luminosity of the quasar, i.e., outflow velocities as high as 4000 km s^{-1} are consistent with the energy balance. This is in contrast with the upper limit on velocity ($v < 1000$ km s^{-1}) by Turner et al. (1993) for NGC 3783, which depended on their assumption of a covering factor of unity. This is unlikely to be applicable to 3C 351 where the covering factor is $\sim$1% (see above). Even for NGC 3783, a covering factor of $\sim$1% would allow for outflow velocities of 3000–4000 km s^{-1} since their limit was based on energy balance requirement that $L_{kinetic} < L_{radiative}$.

Variations in the continuum will change the ionization state of the absorbing gas resulting in corresponding changes in the column densities of individual lines. However, the absorption lines lie on the flat portion of the curve of growth, so a large change in column density would result in a small change in the equivalent widths of the lines. Thus the model predicts no significant correlation between variations in the continuum and the EW of the UV absorption lines. However, a continuum change will result in a change in X-ray opacity and thus in the effective value of U. The signature at the oxygen absorption edge in the X-ray spectrum is predicted to correlate with changes in continuum luminosity.

4. A HIGH-IONIZATION BELR AS THE ABSORBER?

It appears unlikely, based on the results of the previous section, that the absorber can be associated with a BELR cloud. However, given the ambiguity of the BELR covering result and the need for a new population of clouds, we wish to be certain that the BELR is not responsible. Thus we investigate whether the physical characteristics of a BELR cloud are similar to those of the UV/X-ray absorber. Until recently models for the BELR had typical values of the ionization parameter in the line-emitting clouds of $\sim \log U = -2$ (Davidson & Netzer 1978). The value of U for the ionized X-ray absorber in 3C 351 is 100–1000 times larger (Table 1). The line ratio C III] λ1909/C IV λ1549 is a sensitive function of U, and such large values would produce unusually low values for C III]/C IV ($\ll$0.3), and thus it appeared unlikely that a BELR cloud was responsible for the X-ray absorption.

However, in the last few years reverberation studies of a few low-luminosity Seyfert 1 galaxies have revealed that BELR clouds, at least those emitting the high-ionization lines, are closer to the continuum source (lt-days–lt-weeks) and so are exposed to a far more intense radiation field than previously thought (Peterson 1993) with an ionization parameter of $\sim \log U = -0.5$. This result, in combination with the fact that 3C 351 is X-ray–quiet, raises the possibility that BELR clouds could be responsible for the X-ray absorption. These studies have also shown that the C III] λ1909 line, previously used to deduce $n_e \geq 10^9$ cm^{-3}, is formed at a larger distance than the permitted lines (C IV, N V, etc.), $\sim$3–4 lt-weeks (Clavel et al. 1991) and so is produced in different clouds. Thus, there is no clear density indicator for the Lyman α–C IV region. Several implications of this intense radiation at the BELR inner radius are discussed in detail by Ferland & Persson (1980). Of particular relevance to the present study are the following:

1. Free-free heating is more important for higher fluxes or ionization parameters.
2. The strongest effect of the continuum shape is upon the higher ionization lines which are formed near the illuminated face of a cloud.
3. The ratio of C IV λ1549 to Lyα is an increasing function of density because of both the increased free-free heating and the decreased efficiency of Lyα emission.
4. The O VI λ1034 line increases in strength with increasing ionization parameter.

Since the importance of free-free heating increases with the intensity of the incident radiation field, a knowledge of the complete IR–X-ray spectral energy distribution (SED) is needed to understand and model the high ionization emission

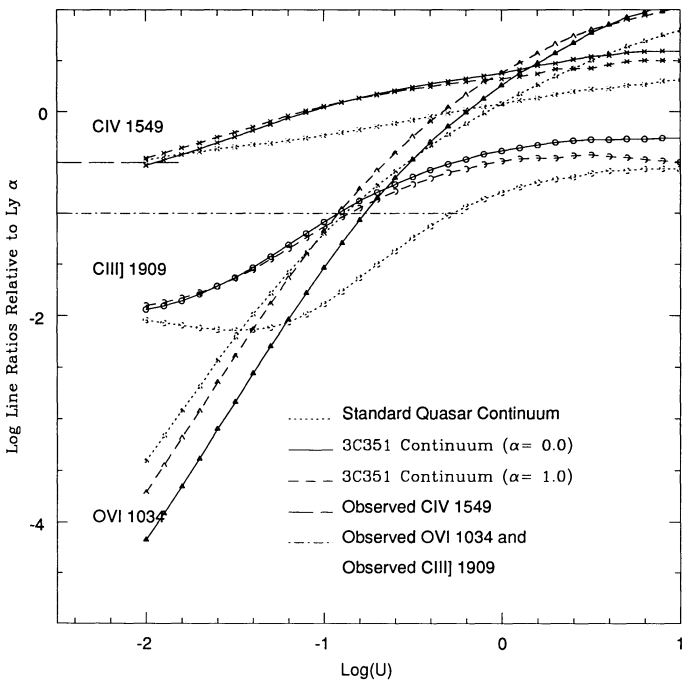

FIG. 5a

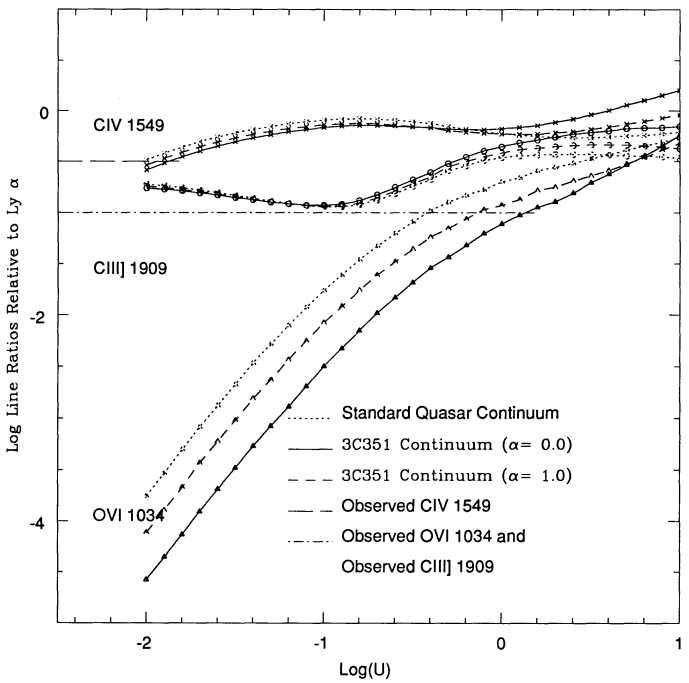

FIG. 5b

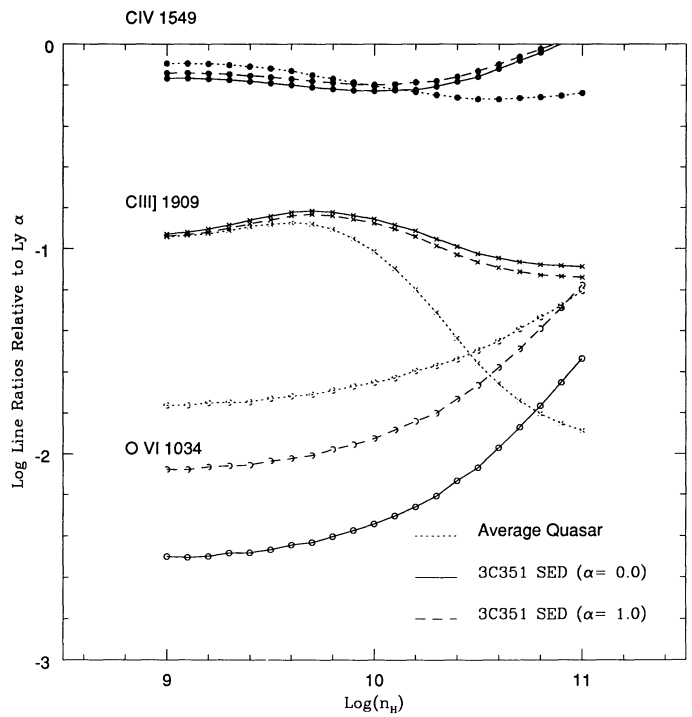

FIG. 5c

FIG. 5.—Line strengths relative to Lyα as a function of (*a*) U for $n_H = 10^{11}$ cm^{-3}, (*b*) for $n_H = 10^9$ cm^{-3}, (*c*) as a function of n_H for log $U = -1.0$ as predicted by photoionization models using the complete observed 3C 351 continuum. Observed values of the line strengths are shown by horizontal lines.

lines. We compared the observed O VI, C IV, and Lyα/N V emission-line EWs with photoionization models to derive the parameters of the emission-line clouds and compared them with the physical parameters of the X-ray/UV absorber. The input spectrum, ionization parameter, hydrogen density, and the column density of a cloud are the physical parameters which uniquely determine the strengths of the emission lines. We have explored a wide range of this parameter space: the hydrogen density was varied between 10^8 and 10^{11} cm^{-3}; Lyman-continuum optical depth: 10^4–10^6; and the ionization parameter log U: -2 to 1; in each case both a standard quasar continuum (Ferland 1991) and the 3C 351 observed continuum were used as input. In the following section we discuss the results.

4.1. *The Effect of the Continuum on the Emission Lines*

The dependence of the emission line strengths measured relative to Lyman-α on the ionization parameter (U) and number density (n_H) is shown in Figures 4 and 5 for all three continua. The effect of the Lyman-continuum optical depth on the line ratios was small (<10%) for optical depths between 10^4 and 10^6. The strongest effect is that using the observed continuum of 3C 351 instead of the standard continuum results in significant changes in the relative emission line strengths (up to a factor of 10).

4.1.1. *The Relation between the Continuum and the Ionization Parameter*

The two extreme wavelength intervals in the 3C 351 continuum, the X-ray and IR-radio, act competitively with opposite effects on the strengths of the emission lines of interest. In Figure 5*a*, C IV, C III], and O VI line strengths relative to Lyα are plotted as a function of U for $n_H = 10^{11}$ cm^{-3}. The larger IR-radio flux in the 3C 351 continuum increases the line ratios due to increased free-free heating. Conversely, the smaller X-ray flux produces lower numbers of ions and decreases the

line ratios. For lower values of U, the low X-ray flux level in the 3C 351 continuum dominates and the line ratios are systematically lower than those produced by the standard continuum. Above some $U_{\rm critical}$ the effect of free-free heating dominates (Fig. 5*a*). The value of $U_{\rm critical}$ is higher for ions with higher ionization potentials and increases with decreasing $n_{\rm H}$; for example $U_{\rm critical}$ for C IV at $n_{\rm H} = 10^{11}$ cm^{-3} is ~ 0.25, whereas for $n_{\rm H} = 10^{9}$ cm^{-3} is ~ 0.63. For low $n_{\rm H}$ ($= 10^{9}$ cm^{-3}), $U_{\rm critical}$ for O VI is sufficiently high that the effect of free-free heating is negligible for almost the entire range of U (Fig. 5*b*).

The strongest effect of the low X-ray flux in 3C 351 is on the strength of the O VI line. This is not surprising since the ionization potential of O V is 0.11 keV. The strength of the O VI line is lower by a factor of ~ 10 with an input spectrum which is X-ray–quiet ($\alpha_{OX} = 1.6$) (Fig. 5*a*). In addition, the low X-ray flux leads to a value of the ionization parameter higher by a factor of 2.5 than that using the standard continuum (Fig. 5*a*). The IR upturn and radio loudness have the opposite effect, but this is significant only when both U and $n_{\rm H}$ are high ($\log U \gtrsim -1$, $n_{\rm H} \sim 10^{11}$ cm^{-3}).

4.1.2. *The Relation between the Continuum and the Density*

When U is low, the shape of the input continuum makes no significant difference to the dependence of emission-line strengths of the C IV and C III] on density, but it always has a significant effect on the dependence of O VI on density. For the standard continuum, the strength of C III] λ1909 drops rapidly for densities higher than the critical density for collisional deexcitation (10^{9} cm^{-3}) (Fig. 5*c*), and so C III] is normally used to put an upper limit on the BELR cloud densities. This effect vanishes using the 3C 351 continuum for high values of U ($\log U > -1$) due to increased free-free heating, which produces heating without ionization. Thus, for a 3C 351–like continuum, i.e., with strong IR emission, C III] λ1909 *ceases to be a density indicator* for $\log U > 0.1$.

Kwan (1984) pointed out that uncertainty in the dielectronic recombination rates and the strong dependence of C III] λ1909/C IV λ1549 on U compromised its role as a density indicator. Our results show a second reason to discount the value of C III] as a density diagnostic. We conclude that, even without variability information to confirm C III]'s origin in different gas, it is not a good indicator of density in the high-ionization Lyα–C IV–emitting region.

4.2. *Comparison with Observations*

To investigate whether the physical parameters of BELR clouds are the same as those of the warm absorber, we compared the photoionization model calculations described above with the observed emission lines C III], C IV, O VI, and Lyα. The observed strength of C III] λ1909 relative to Lyα ($= 0.1$) is used only as an upper limit in this comparison because, as discussed earlier, it is believed to originate in a separate, larger region than the C IV–O VI–producing clouds. As shown in Figure 5*b*, this constraint is not satisfied for low densities ($n_{\rm H} = 10^{9}$ cm^{-3}) for the entire range of U. Even for higher densities (Fig. 5*a*, $n_{\rm H} = 10^{11}$ cm^{-3}), the constraint is satisfied only for $\log U < -1.2$, lower than that required for O VI production, i.e., no consistent result can be found.

The large predicted strength of C III] results from the large amount of free-free heating due mainly to the IR upturn in the 3C 351 continuum. If this IR is produced by thermal emission from dust at larger distances from the nucleus, instead of in the central region, the BELR clouds will see much weaker IR flux, reducing the free-free heating. In this scenario, we compared the observed line ratios of C IV/Lyα and O VI/Lyα with those predicted by the 3C 351 continuum without the IR upturn (Fig. 6). The C III] line constraint is now satisfied for the range of U relevant for the C IV–O VI producing clouds (up to $\log U \sim -0.2$, for $n_{\rm H} = 10^{11}$ cm^{-3}). If C III] is produced predominantly at a distance larger than the C IV–Lyα clouds, then the IR upturn is necessarily produced beyond the BELR clouds arguing in favor of a dust model for the IR emission (Sanders et al. 1989; Barvainis 1993).

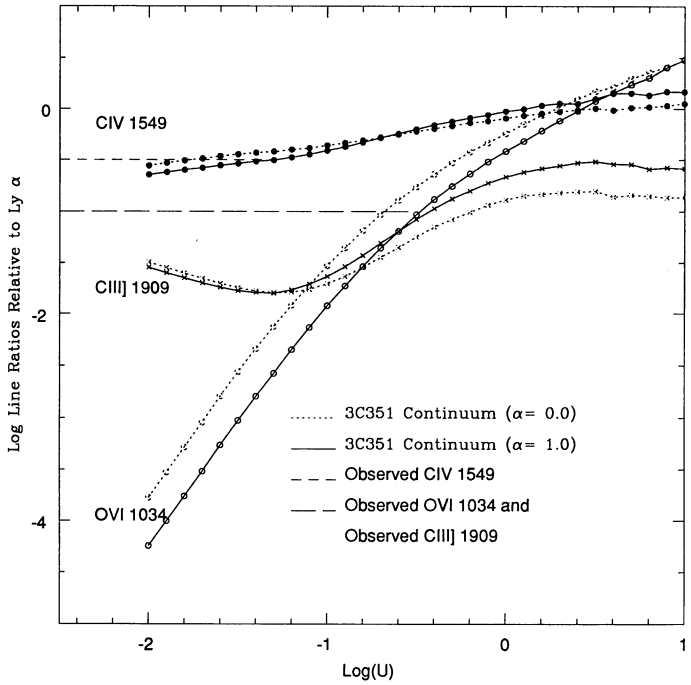

FIG. 6.—Line strengths relative to Lyα + N V as a function of U for $n_{\rm H} = 10^{11}$ cm^{-3}. The 3C 351 continuum here is that without either the IR upturn or radio (see § 4.2). Observed values of the emission lines are shown by horizontal lines.

The observed C IV/Lyα ratio give a value of the ionization parameter for C IV–Lyα–producing clouds of $\log U = -1.5 \pm 0.2$ for $n_{\rm H} = 10^{11}$ cm^{-3} (Fig. 6). The inferred value for O VI λ1034 is much larger, $\log U = -0.6 \pm 0.1$, implying that O VI is produced closer to the ionizing continuum than the C IV–Lyα clouds. Even though this U is much larger than the standard value ($\log U = -0.5$ as compared to -2) (Fig. 6), it is still much lower than that required for the X-ray absorber ($\log U = 0.78$–1.08). Thus, we rule out the possibility of identifying the X-ray absorber as a BELR cloud.

It is still possible that the BELR clouds provide the parent population for the outflowing absorption line clouds. We discuss this possibility further in section 5.2.

5. ARE THERE OTHER UV/X-RAY ABSORBERS?

5.1. *Previous Studies*

Strong, associated metal line absorption has been observed before in AGNs with soft X-ray absorption. However, in no case was the UV absorber identified with the X-ray absorber as the physical parameters of the two were deduced to be very different. Our results for 3C 351 show that there are five reasons for these apparently discrepant conditions:

1. The Mg II ion is not produced in enough abundance until

column densities are high (Kwan & Krolik 1981), so the absence of Mg II absorption in a high-ionization absorption system was interpreted as due to a low ($N_H < 10^{20.5}$) column density. However, the column densities inferred from the X-ray data were some two orders of magnitude higher ($N_H \sim 10^{22}$–10^{23}) and thus completely inconsistent. Our analysis shows that the reason for the lack of Mg II absorption may instead be that the material is highly ionized. In this case large column densities are allowed despite the absence of Mg II absorption as magnesium is predominantly in high-ionization states.

2. A second consequence of the assumed low column densities for the UV absorbers is that the absorbing gas would be fully ionized (Shull & Sachs 1993) in hydrogen. In our analysis the column densities are large enough to allow partial ionization and hence the Lyα absorption.

3. The key high-ionization line O VI λ1034 is not easily observed in AGNs with *IUE*. It can only be seen for $z \gtrsim 0.2$, and few AGNs at such redshift are bright enough to be studied with *IUE*. C IV was thus the most commonly observed high-ionization absorption line. For optically thin, AGN-photoionized gas, C IV is the dominant carbon ionization state when $\log U \sim -2.3$ (Donahue & Shull 1991). Since strong C IV absorption was observed, such values were assumed to be appropriate for the UV absorber. This is much lower than that required for a warm absorber. However the combination of C IV and O VI absorption in 3C 351 demonstrates that this assumption does not apply. In the present model the ionization parameter of the absorber is high ($\log U \sim 0.78$), and C VI rather than C IV is the dominant state of ionization.

4. Early X-ray observations constrained only the total absorbing column density along the line of sight due to either a lack of sensitivity below the 0.6 keV oxygen edge, or of resolution to detect the edge. Absorption as seen in the X-rays was assumed to be due to neutral, "cold" gas because "hot" gas would be transparent to X-rays. There was no observational constraint on the actual ionization structure of the absorber. The higher spectral resolution of *ROSAT* allows detection of absorption edges, thus constraining the ionization state of the absorber and providing clear evidence for partially ionized gas.

5. The physical conditions of the absorbing gas are poorly determined from absorption line studies in the UV alone (Lanzetta et al. 1991) because only a few lines are measured (N V λ1240, C IV λ1549, and possibly Mg II λ2798 or O VI λ1034) yielding column density estimates of a few ions but no information on the ionization state. Since the X-ray absorption cross section is relatively insensitive to ionization and depletion (Morrison & McCammon 1983), X-ray measurements give a total column density.

We have now demonstrated that the combination of UV and X-ray provides information on the ionization state of the gas and hence the physical conditions.

The case of the Seyfert galaxy NGC 3516 ($z = 0.009$) is instructive. Kolman et al. (1993) present simultaneous X-ray and UV observations of NGC 3516 with absorption features seen in the UV spectrum and the signature of a warm absorber in the X-ray spectrum. The authors rule out a common origin of the UV and X-ray absorption.

The X-ray observations were made with *Ginga* which has its response at higher energies (1–20 keV) than *ROSAT* (0.1–2 keV). The warm absorber in NGC 3516 has an absorption edge in the range 7.4–8.3 keV, which includes ionization stages from Fe^{+12} to Fe^{+21}. A simple warm absorber model was constructed by introducing an additional absorption edge in to the model; a physical warm absorber was not constructed, and thus U could not be constrained. The UV spectrum from *IUE* contains absorption lines of C IV, N V, and Si IV and the low-ionization line Mg II. U was deduced by assuming that the fractional abundance of C IV is a maximum yielding a low value of U ($\log U = -2.18$ to -0.83 for $\log N_H = 20$–22). In the warm absorber, iron is at least 12 times ionized, which is consistent with C^{+5} and higher stages of ionization. Therefore, such matter is probably too highly ionized to produce the observed UV absorption lines, especially Mg II; hence their conclusion that the absorbers were distinct. However, we note that the evidence for Mg II absorption in NGC 3516 is rather weak (Kolman et al. 1993) due to blending with a Galactic absorption line. If this line is not confirmed (e.g., in an *HST* spectrum), then highly ionized matter similar to that in 3C 351 is a possibility. It may then be possible to reconcile the ionization states of the UV and X-ray absorbers in NGC 3516.

5.2. *Implications*

The identification of the UV and X-ray absorbers in 3C 351 with the same absorbing gas opens up many possibilities. We note, for example, that if the clouds are expanding laterally at their sound speeds, then the ionization parameter of the clouds would change as they flow out with $U \propto R(v_{sound}/v_{outflow})^3$. Projecting the cloud density and U back to the radius of the BLR gives values consistent within a factor of 2 with those for the BELR clouds, so that the outflow may be built from outflowing BELR material. These clouds could attain velocities an order of magnitude larger without disrupting the energy balance (see § 3.2), which would then give them properties closely similar to the BAL outflows (Turnshek 1988). BALQSOs typically have $N_H \sim 10^{21-22}$ cm^{-2}, are highly ionized and have a complex velocity structure. Initial results from *ROSAT* (Kopko, Turnshek, & Espey 1993) imply that they are relatively faint in soft X-rays, suggestive of strong absorption and another UV/X-ray absorber connection. Cold, yet variable, absorbers are quite common in the X-rays (Turner & Pounds 1989; Warwick et al. 1993). If we assume that these absorbers are related to the UV/X-ray ionized absorbers only denser, or more distant so that they have lower U, then we can begin to make progress in understanding them. This is shown to be the case in 3C 212 which was originally thought to be a cold absorber (Mathur 1994). Presently these absorbers are usually associated with the "obscuring tori" indicated in unified schemes (e.g., Antonucci & Miller 1985). Identification with the kind of outflow seen here suggests a more dynamic "expanding shell" picture (see also Lawrence 1991). Once again the combination of UV and X-ray data would result in strong constraints on the physical conditions of the absorber.

6. CONCLUSIONS

In this paper we have shown that the X-ray and UV absorbers in 3C 351 are highly likely to be one and the same. The physical conditions of the absorber are determined through the combination of constraints derived from both the X-ray and UV analysis. The absorber is found to be highly ionized ($\log U = 0.78$–1.08), outflowing with a velocity $\sim$3050 km s^{-1}, having high column density ($N_H = 1$–2×10^{22} cm^{-2}), low density ($n \lesssim 10^7$ cm^{-3}); probably a low covering factor ($\sim$1%) and situated outside the BELR. These properties

describe a component of the active nucleus not previously recognized.

This is the first confirmed X-ray/UV absorber. We have shown that the previous attempts to identify an UV absorber with a X-ray absorber were unsuccessful because of the lack of high-quality data which forced overly constraining assumptions to be made in photoionization modeling. These led to incompatible conditions being derived for the UV and X-ray absorbers. The identification of the UV and X-ray absorbers in 3C 351 with the same absorbing gas opens up new possibilities for studying the physical conditions in other UV and X-ray absorbers, e.g., BALQSOs. We have demonstrated the great advantage in determining the properties of the absorber that is afforded by the combination of UV and X-ray data.

We have also investigated the effect of the 3C 351 continuum on emission-line strengths. The 3C 351 continuum differs significantly from the standard continuum in that it is X-ray–quiet, radio-loud, and has an upturn in the IR. We demonstrate that it is important to use observed continuum, rather than a standard one, to derive the physical parameters in the BELR self-consistently. The strongest effect of the low X-ray flux is on the strength of O VI λ1034. The strengths of the high-ionization lines of C IV λ1549 and O VI λ1034 with respect to Lyα are systematically lower (up to a factor of 10) with the 3C 351 continuum as compared to those produced by the standard continuum for $U < U_{\rm critical}$. This is mainly due to the weak X-ray flux. Free-free heating was found to be important for large values of the ionization parameter ($\log U > -1$) and higher densities ($n \sim 10^{11}$ cm^{-3}). We find that for a 3C 351–like (IR-strong) continuum, C III] λ1909 ceases to be a density indicator if the BELR gas sees the same continuum. We rule out the identification of the absorber with a BELR cloud as the physical conditions in the two regions are inconsistent with one another. It is possible that the BELR clouds provide the parent population for the outflowing absorption-line clouds.

3C 351 was observed by us with *ROSAT* because it was known to be X-ray–quiet, as a part of our program to observe quasars with extreme continuum properties. Our expectation was that they would produce new insights into the underlying physical processes. This strategy indeed seems to be fruitful.

We thank the Quasar Absorption Line Key Project team for making the *Hubble Space Telescope* observations available. We acknowledge the Data Management Facility/Data Archiving and Distributing System (DMF/DADS) at STScI for making the archived *IUE* Quasar Atlas available. We thank T. Kallman, H. Netzer, A. Dobrzycki, and J. McDowell for useful discussions; B. Jannuzi for help with the *HST* spectra; and G. Ferland for providing us with the photoionization code CLOUDY.

This work was supported by NASA grants NAGW-2201 (LTSA), NASA 5-30934 (RSDC), and NAG 5-1883 (*ROSAT*).

REFERENCES

Antonucci, R. R. J., & Barvainis, R. 1988, ApJ, 325, L21
Antonucci, R. R. J., & Miller, J. S. 1985, ApJ, 297, 621
Bahcall, J. N., et al. 1993, ApJS, 87, 1
Barvainis, R. 1993, ApJ, 412, 513
Boissé, O., Boulde, D., Kunth, D., Tytler, D., & Vigroux, L. 1992, A&A, 262, 401
Chini, R., Kreysa, E., & Biermann, P. L. 1989, A&A, 219, 87
Clavel, J., et al. 1991, ApJ, 366, 64
Davidson, K., & Netzer, H. 1979, Rev. Mod. Phys., 51, 715
Donahue, M., & Shull, J. M. 1991, ApJ, 383, 511
Ellingson, E., Yee, H. K. C., Bechtold, J., & Dobrzycki, A. 1994, ApJ, submitted
Elvis, M., et al. 1994, ApJS, in press
Espey, B. R., Carswell, R. F., Bailey, J. A., Smith, M. G., & Ward, M. J. 1989, ApJ, 342, 666
Ferland, G. F. 1991, "HAZY" (OSU Astronomy Department Internal Report)
Ferland, G. F., & Persson, S. E. 1989, ApJ, 347, 656
Fiore, F., Elvis, M., Mathur, S., Wilkes, B., & McDowell, J. 1993, ApJ, 415, 129 (Paper I)
Grevesse, N., & Anders, E. 1989, in Abundances of Matter, ed. C. J. Waddington (New York: AIP)
Kinney, A. L., Bohlin, R. C., Blades, J. C., & York, D. G. 1991, ApJS, 75, 645
Kolman, M., Halpern, J. P., Martin, C., Awaki, H., & Koyama, K. 1993, ApJ, 403, 592
Kopko, M., Turnshek, D. A., & Espey, B. 1993, in IAU Symp. 159, Quasars Across Electromagnetic Spectrum, ed. T. J.-L. Courvoisier & A. Blecha (Dordrecht: Kluwer), 450
Kwan, J. 1984, ApJ, 283, 70
Kwan, J., & Krolik, J. H. 1981, ApJ, 250, 478
Lanzetta, K. M., Wolfe, A. M., Turnshek, D. A., Lu, L., McMahon, R. G., & Hazard, C. 1991, ApJS, 77, 1
Lawrence, A. 1991, MNRAS, 252, 586
Mathews, W. G., & Ferland, G. J. 1987, ApJ, 323, 456
Mathur, S. 1994, ApJ, 431, L75
Morrison, R., & McCammon, D. 1983, ApJ, 270, 119
Peterson, B. M. 1993, PASP, 105, 247
Sanders, D., Phinney, E. S., Neugebauer, G., Soifer, B. T., & Matthews, K. 1989, ApJ, 347, 29
Schneider, D. P., et al. 1993, ApJS, 87, 45
Shastri, P., Wilkes, B. J., Elvis, M., & McDowell, J. C. 1993, ApJ, 410, 29
Shull, J. M., & Sachs, E. R. 1993, ApJ, 416, 536
Spitzer, L. 1978, Physical Processes in the Interstellar Medium (New York: Wiley-Interscience)
Turner, T. J., Nandra, K., George, I. M., Fabian, A., & Pounds, K. A. 1993, ApJ, 419, 127
Turner, T. J., & Pounds, K. A. 1988, MNRAS, 232, 463
———. 1989, MNRAS, 240, 833
Turnshek, D. A. 1988, in QSO Absorption Lines: Probing the Universe, ed. J. C. Blades, D. Turnshek, & C. A. Norman (Cambridge: Cambridge Univ. Press), 17
Ulrich, M. H. 1988, MNRAS, 230, 121
Warwick, R., Sembay, S., Yaqoob, T., Makishima, K., Ohashi, T., Tashiro, M., & Kohmura, Y. 1993, MNRAS, 265, 412
Wiese, W. L., Smith, M. W., & Glennon, B. M. 1966, Atomic Transition Probabilities (Washington: US Government Printing Office)
Wilkes, B. J., & Elvis, M. 1987, ApJ, 323, 243
Wilkes, B. J., Tananbaum, H., Worall, D. M., Avani, Y., Oey, M. S., & Flanagan, J. 1994, ApJS, in press